

## Electrochemical studies of two pyrrolo[1,2-*c*]pyrimidines

M.-L. Tatu<sup>1</sup>, F. Harja<sup>1</sup>, E.-M. Ungureanu<sup>1\*</sup>, E. Georgescu<sup>2</sup>, L. Birzan<sup>3</sup>, M.-M. Popa<sup>3</sup>

<sup>1</sup>Department of Inorganic Chemistry, Physiscal Chemistry and Electrochemistry, University "Politehnica" of Bucharest, Gh. Polizu 1-7, 011061, Romania

<sup>2</sup>Research Center Oltchim, Uzinei Street 1, 240050, Ramnicu Valcea, Romania,

<sup>3</sup>Romanian Academy, Institute of Organic Chemistry "C. D. Nenitzescu", Spl. Independentei, 202B, 060023-Bucharest, 35 P.O. Box 108, Romania

Received August 25, 2017; Accepted September 18, 2017

The electrochemical characterization of two pyrrolo[1,2-*c*]pyrimidines has been performed by cyclic voltammetry (CV), differential pulse voltammetry, and rotating disk electrode voltammetry. Their diffusion coefficients were determined from the scan rate influence on CV anodic currents. Modified electrodes were prepared in pyrrolo[1,2-*c*]pyrimidines solutions in acetonitrile containing tetrabutylammonium perchlorate by cycling the potential or by controlled potential electrolysis at different anodic potentials and charges.

**Keywords:** pyrrolo[1,2-*c*]pyrimidines, cyclic voltammetry, differential pulse voltammetry, diffusion coefficients, modified electrodes, rotating disk electrode

### INTRODUCTION

The pyrrolo[1,2-*c*]pyrimidine type structures are present in many natural products [1-6], and these compounds have been studied for their bioactivity. Some compounds of this class have antioxidant, antifungal and antimicrobial properties, or are used in cancer treatments. Pyrrolopyrimidine derivatives are used for their PI3Ka kinase inhibitory activity, for the treatment of MDR pathogens [6-10].

Pyrrolo[1,2-*c*]pyrimidine is an N-bridgehead heterocyclic compound obtained by formal condensation of a pyrrole with a pyrimidine [9]. Different procedures for the synthesis of pyrrolo[1,2-*c*]pyrimidines starting from suitable substituted pyrroles [10-11] or pyrimidines [12-15] are described. The reactions starting from different pyrrole structures such as pyrrole-2-carboxaldehyde with tosylmethyl isocyanide gives pyrrolo[1,2-*c*]pyrimidine derivatives with a good yield, but they use the hazardous isocyanide derivative, and the tosyl group cannot be removed so easy. Thus, the most efficient and environmentally friendly method to obtain pyrrolo[1,2-*c*]pyrimidines is by 1,3-dipolar cycloaddition reaction of the pyrimidinum *N*-ylides in 1,2-epoxybutane as reaction medium. The use of the epoxide as a reaction medium and acid scavenger has the advantage of direct formation of the final compound avoiding the generation of the inactivated product [9, 16-21].

There are several studies on the electrochemical characterization of pyrrolo[1,2-*c*]pyrimidine

derivatives reported by our group [22]. Their characterization has been done by cycling voltammetry (CV), and differential pulse voltammetry (DPV). The present paper is focused on the electrochemical characterization of two other related pyrrolo[1,2-*c*]pyrimidines. The electrochemical study is important as it offers the simplest method to estimate HOMO and LUMO energies of a molecule [23], which is essential for organic light-emitting diode (OLED) applications.

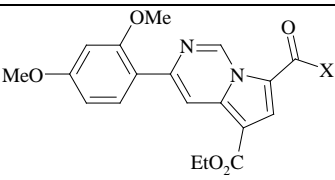
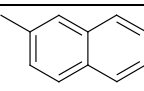
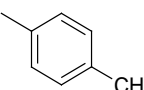
The two compounds are ethyl3-(2,4-dimethoxyphenyl)-pyrrolo[1,2-*c*]pyrimidine-5-carboxylates substituted at position 7 of the pyrrole ring either with 2-naphthoyl (**P1**) or with 4-methylphenylcarbonyl (**P2**). CV, DPV and also rotating disk electrode (RDE) voltammetry have been used for their characterization. Modified electrodes have been obtained by potentiodynamic or potentiostatic methods in order to future applications.

### EXPERIMENTAL

The pyrrolo[1,2-*c*]pyrimidines were synthesized as previously described [20-22]. The structure and melting point (m.p.) of compounds considered in the present study are given in Table 1. Their electrochemical study was performed in acetonitrile (CH<sub>3</sub>CN) in the presence of tetrabutylammonium perchlorate (TBAP), both from Fluka.

\* To whom all correspondence should be sent.  
E-mail: ungureanu2000@yahoo.com

**Table 1.** Investigated pyrrolo[1,2-c]pyrimidines

Formula	Entry	X	m.p. (°C)
	<b>P1</b>		163-164
	<b>P2</b>		230-231

PGSTAT 12 AUTOLAB potentiostat connected to a three-electrode cell was used for electrochemical investigation. A glassy carbon electrode disk (3 mm diameter) from Metrohm was used as working electrode. Its active surface was polished with diamond paste (2  $\mu\text{m}$ ) and cleaned with the acetonitrile before each experiment. Ag/10 mM AgNO<sub>3</sub> in 0.1 M TBAP/CH<sub>3</sub>CN was used as reference electrode. The auxiliary electrode was a platinum wire. The experiments were performed at room temperature (25°C) under argon atmosphere. All potentials were referred to the potential of ferrocene/ferrocenium redox couple (Fc/Fc<sup>+</sup>) which in our experimental conditions was +0.07 V. CV curves were usually recorded at 0.1 V·s<sup>-1</sup> or at various scan rates (0.1 – 1 V·s<sup>-1</sup>), DPV curves at 0.01 V·s<sup>-1</sup> with a pulse height of 0.025 V and a step time of 0.2 s, and RDE curves at 0.01 V·s<sup>-1</sup>

## RESULTS AND DISCUSSIONS

The electrochemical characterization was performed in millimolar solutions of each

pyrrolo[1,2-c]pyrimidine by CV, DPV, and RDE at different concentrations in 0.1 M TBAP/CH<sub>3</sub>CN. All anodic and cathodic curves were recorded starting from the stationary potential. In all cases, the processes put in evidence by DPV were denoted in the order of their apparition in DPV curves in anodic (a1, a2, ...) or cathodic (c1, c2, ...) scans, and this notation was kept for the corresponding processes recorded by other methods (CV or RDE).

### Study of P1

DPV and CV curves at different concentrations (0 – 0.75 mM) of **P1** are presented in Figure 2. The DPV curves show four anodic (a1 – a4), and four cathodic peaks (c1 – c4). They highlight, respectively, 4 oxidation and 4 reduction processes which can occur during the potential scans. The peaks are also seen in CV curves. CV anodic peaks are less prominent, due to the superposition to the background oxidation process (dotted line). The peak currents increase with concentrations for CV and DPV curves.

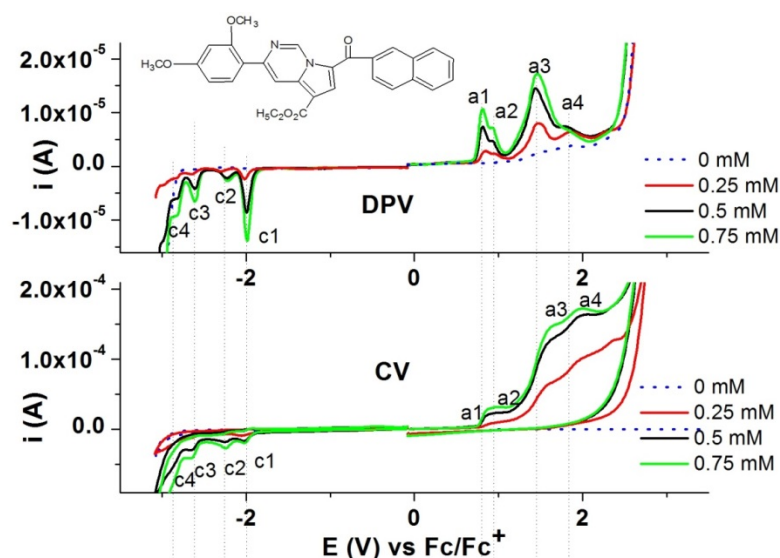


**Fig.2.** CV (0.1 V·s<sup>-1</sup>) and DPV (0.01 V·s<sup>-1</sup>) curves on glassy carbon electrode (diameter 3 mm) at different concentrations for **P1** in 0.1 M TBAP/CH<sub>3</sub>CN

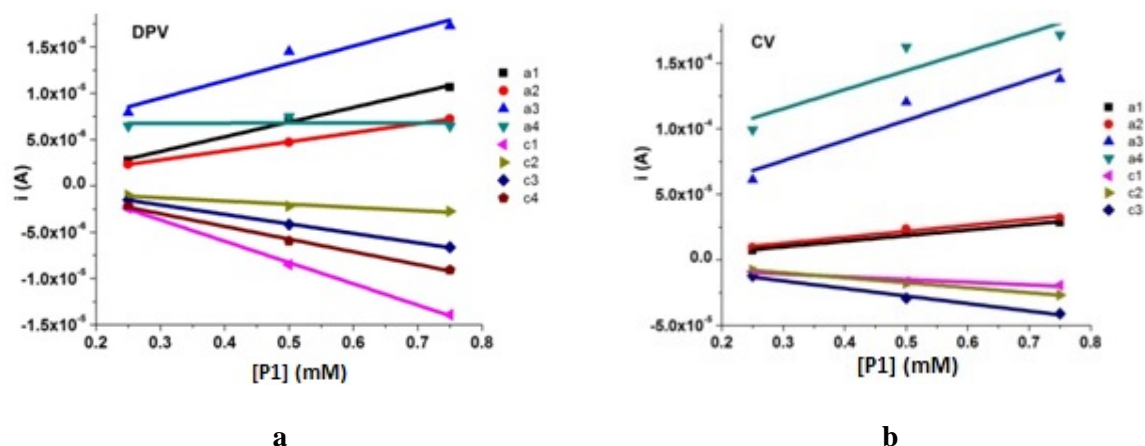


**Fig. 3.** Linear dependences of the peak currents on concentration from DPV ( $0.01 \text{ V}\cdot\text{s}^{-1}$ ) (a) and CV ( $0.1 \text{ V}\cdot\text{s}^{-1}$ ) (b) curves from Fig. 2

**Table 2.** Equations and the correlation coefficients of the linear peak currents dependences on **P1** concentration\* from CV ( $0.1 \text{ V}\cdot\text{s}^{-1}$ ) and DPV ( $0.01 \text{ V}\cdot\text{s}^{-1}$ ) curves from Fig. 3

Method	Equation	Correlation coefficient
DPV	$i_{\text{peak a1}} = -1.03 + 15.86 \cdot [\text{P1}]$	0.984
	$i_{\text{peak a2}} = -0.14 + 9.81 \cdot [\text{P1}]$	0.998
	$i_{\text{peak a3}} = 3.86 + 18.75 \cdot [\text{P1}]$	0.896
	$i_{\text{peak c1}} = 3.22 - 22.99 \cdot [\text{P1}]$	0.997
	$i_{\text{peak c2}} = -0.22 - 3.49 \cdot [\text{P1}]$	0.905
	$i_{\text{peak c3}} = 1.02 - 10.24 \cdot [\text{P1}]$	0.999
	$i_{\text{peak c4}} = 1.11 - 13.72 \cdot [\text{P1}]$	0.994
CV	$i_{\text{peak a1}} = -3.02 + 42.94 \cdot [\text{P1}]$	0.972
	$i_{\text{peak a2}} = -1.05 + 45.48 \cdot [\text{P1}]$	0.960
	$i_{\text{peak a3}} = 29.53 + 153.78 \cdot [\text{P1}]$	0.821
	$i_{\text{peak c1}} = 1.83 - 24.58 \cdot [\text{P1}]$	0.971
	$i_{\text{peak c2}} = 1.57 - 38.07 \cdot [\text{P1}]$	0.997
	$i_{\text{peak c3}} = 1.15 - 57.46 \cdot [\text{P1}]$	0.979

\* $i_{\text{peak}}$  is expressed in  $\mu\text{A}$ , and  $[\text{P1}]$  in  $\text{mmol}\cdot\text{l}^{-1}$

The linear dependences of the total currents vs concentration for DPV and CV curves are presented in Figure 3a and 3b, respectively. Table 2 shows the equations and the correlation coefficients for these linear dependences of all peak currents on **P1** concentration. The slopes in Table 2 show the increase in peak height with the **P1** concentration. It occurs with different slopes for the investigated peaks, indicating a complexity of the involved processes. It can be seen that peak a3 has a correlation coefficient less than 0.9, both in DPV and in CV. The peak potentials from DPV and CV curves for **P1** are given in Table 3.

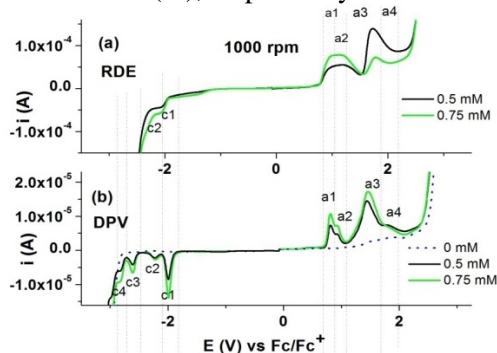
RDE anodic and cathodic curves at various concentrations (0.25 – 0.75mM) are given in Fig. 4 for a constant rotation rate (1000 rpm) and in Fig. 5 for different rotation rates (500 – 2000 rpm) at constant concentration (0.5 mM) of **P1**. The DPV curves for this concentration are presented

underneath, in order to allow their parallel evaluation.

From Figs. 4 and 5 it can be seen that RDE cathodic currents have regular behaviour (increasing with **P1** concentration and rotation rate of the electrode). Conversely, the anodic currents have particular variation: they are increasing with concentration for RDE anodic wave corresponding to a1 process, while in the range of a2 DPV peak, the current promptly decreases to the background value and it increases again in the range of a3 process, but not proportionally. The isosbestic point is situated at about 1.53 V. There is no wave corresponding to a4 DPV peak on RDE curves.

The anodic curves for **P1** could be explained by the processes given in Table 3. After **P1** oxidation to the radical cation (peak a1), there is an irreversible process of film formation in the range of a2 peak, which continues at more positive potentials. In the

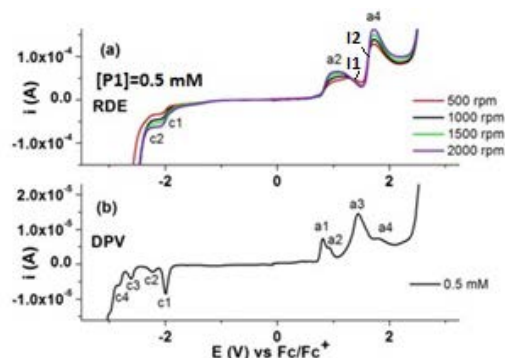
range of a3, there is another oxidation process, which competes with the film formation started in a2. It has the highest current at the smallest concentration of **P1**. These aspects are in agreement with the RDE curves in Fig. 5. When increasing the rotation rate of RDE, only the currents for anodic a1 and a4 peaks are increasing. The currents for a2 are constant, while those for a3 are decreasing. This means these processes (a1, a4) are not involved in the film formation, as it is the case for a2. The currents for a3 are inversely proportional to the imposed rotation rate. At low rotation rates, the current in the domain of a3 is higher, as the intermediates for the film formation can stay close to the electrode and keep on the polymerization process. Two isosbestic points which delimitates the change between processes can be noticed at 1.299 V (I1) and 1.627 V (I2), respectively.



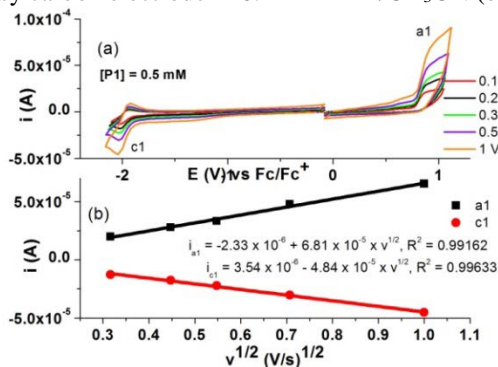
**Fig. 4.** RDE curves (0.01 V·s<sup>-1</sup>) on glassy carbon electrodes (3 mm diameter) at different concentrations in **P1** solution in 0.1 M TBAP/CH<sub>3</sub>CN at 1000 rpm (a), DPV curves (0.01 V·s<sup>-1</sup>) obtained for **P1** on glassy carbon electrode (3 mm diameter) in 0.1 M TBAP/CH<sub>3</sub>CN (b)

Figure 6 presents the CV curves in the range of the first anodic and cathodic peaks for **P1** (0.5 mM) at different scan rates, and the dependences of the total peak currents for a1 and c1 peaks vs the scan rate. It can be seen that the total currents linearly increase with the square root of the scan rate (with good correlation coefficients for a1 and c1). It can be seen also from Fig. 6a that a1 is an irreversible process, while c1 is a quasi-reversible process, having a corresponding peak in the reverse scan c1' situated at about 100 mV vs c1.

In figure 7 are given the CV curves for **P1** (0.5 mM) on different scan domains. From these curves, the reversibility of each process in the anodic and cathodic domains has been estimated. Processes obtained in the anodic domains are irreversible, while the cathodic ones are reversible or quasi-reversible (Table 3), the last mentioned showing corresponding peaks situated at potentials of less than 100 mV in respect with the peaks in the direct scans.



**Fig. 5.** RDE curves on glassy carbon electrode (3 mm diameter) in **P1** solution (0.5 mM) in 0.1 M TBAP/CH<sub>3</sub>CN at different rotation rates (500 – 2000 rpm) (a), and DPV curve (0.01 V·s<sup>-1</sup>) for **P1** (0.5 mM) on glassy carbon electrode in 0.1 M TBAP/CH<sub>3</sub>CN (b)



**Fig.6.** CV curves in 0.1 M TBAP/CH<sub>3</sub>CN on glassy carbon electrode (3 mm diameter) for **P1** (0.5 mM) at different scan rates (0.1 – 1 V·s<sup>-1</sup>) (a) and dependences of the peak currents on the square root of the scan rate (b)

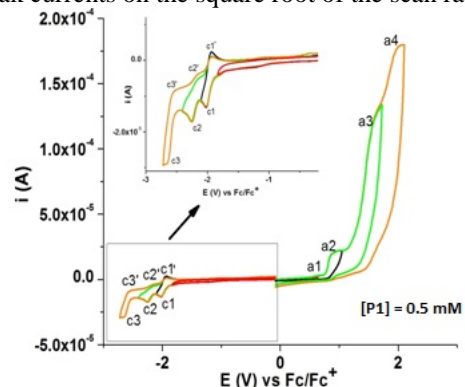


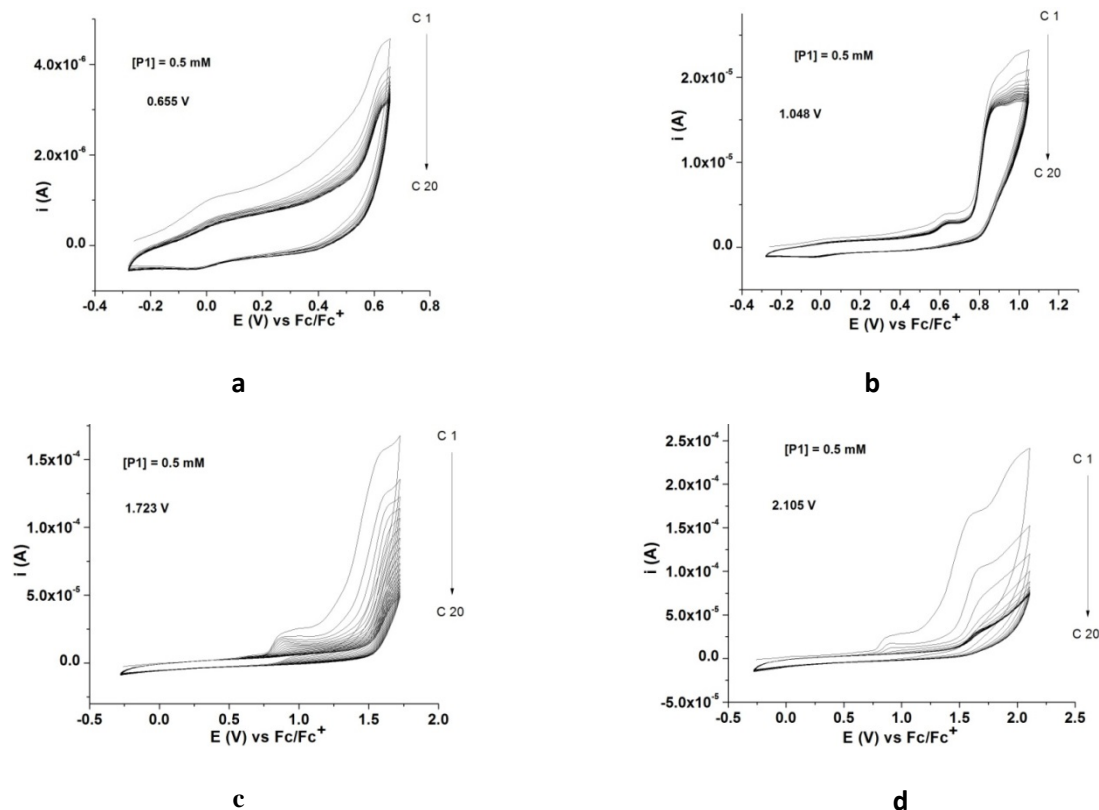
**Fig.7.** CV curves (0.1 V·s<sup>-1</sup>) at different scan domains on glassy carbon electrode (3mm diameter) for **P1** (0.5 mM) in 0.1 M TBAP/CH<sub>3</sub>CN; inset A: detail of the cathodic domain

### Modified electrodes based on **P1**

Chemical modified electrodes (CME) based on electrode coverage with compound **P1** were obtained either by potentiodynamic (successive scans) or potentiostatic (controlled potential electrolysis) methods in solutions of **P1**(0.5 mM) in the domain of the anodic processes a1, a2, a3, and a4.

**Table 3.** Peak potential values (V) vs Fc/Fc<sup>+</sup> for **P1** from DPV and CV curves

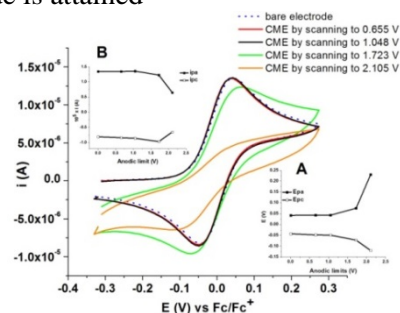
Peak	Method		Process characteristic
	DPV	CV	
a1	0.81	0.86	irreversible
a2	0.93	0.97	irreversible
a3	1.44	1.57	irreversible
a4	1.80	1.98	irreversible
c1	-1.99	-2.03	reversible
c2	-2.23	-2.26	quasi-reversible
c3	-2.61	-2.65	quasi-reversible
c4	-2.82	-	quasi-reversible



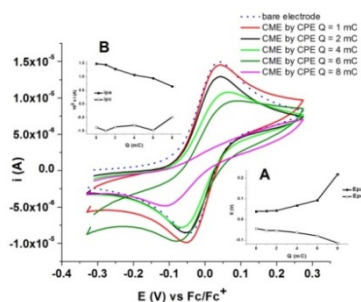
**Fig. 8 .** CV curves (0.1 V·s<sup>-1</sup>) during the preparation of CME by successive scans in 0.5 mM solution of **P1** in 0.1 M TBAP/CH<sub>3</sub>CN between -0.3 V and different anodic limits: +0.655 V (a); +1.048 V (b); +1.723 V (c); +2.105 V (d)

Figure 8 presents the CV curves during the preparation of CME by potentiodynamic method. Figure 9 shows the CV curves obtained after the transfer of the modified electrodes obtained by successive potential scans between -0.3 V and different anodic potentials (+0.655 V (Fig. 8a); +1.048 V (Fig. 8b); +1.723 V (Fig. 8c); +2.105 V (Fig. 8d)) in 1 mM ferrocene solution in 0.1 M TBAP/CH<sub>3</sub>CN. The ferrocene CV curves obtained on CMEs are different than the CV curve obtained for the bare electrode. In the inset A are the dependences of the anodic and cathodic peak potentials for ferrocene (Fc) on the anodic limit scan, that show important variations starting at potentials more positive than 1.5 V. In the inset B are shown the corresponding anodic and cathodic currents dependencies, which have the same behavior as those shown by inset A. It can be seen

that the ferrocene signal is the most diminished for the potential scan limit of +2.105 V, where it can be assumed that the most compact coverage of the electrode is attained



**Fig. 9.** CV curves (0.1V/s) for CME prepared by successive scans (in 0.5 mM solution of P1 in 0.1 M TBAP/CH<sub>3</sub>CN) after the transfer of CME in 1mM Fc solution in 0.1 M TBAP, CH<sub>3</sub>CN; dependences of the anodic and cathodic Fc peak potentials (inset A) and currents (inset B) on the anodic limit



**Fig. 10.** CV curves (0.1V/s) for CME prepared by CPE (at +2.105 V in 0.5 mM solution of **P1** in 0.1 M TBAP/CH<sub>3</sub>CN) after the transfer of CME in 1mM Fc solution in 0.1 M TBAP, CH<sub>3</sub>CN; dependences of the anodic and cathodic Fc peak potentials (inset A) and currents (inset B) on electropolymerization charge (Q)

Films based on **P1** have been also prepared by CPE at different potentials: 0.655V, 1.048 V, 1.723 V, 2.105 V using a charge of 1 mC. The CV curves of the CMEs in transfer ferrocene solution have very small changes in respect with the bare electrode, indicating a weak coverage of the electrode. However, the CPE performed at 2.105 V led to evident changes which occur continuously when the charge increases from 1 mC to 8 mC. In Fig. 10 are given the CV curves after the transfer in ferrocene solution of the CMEs obtained at 2.105 V, indicating the continuous increase of the coverage of the electrode. For the potential of +2.105 V the most insulating film is obtained at 8 mC, for which the ferrocene curve has the smallest anodic peak, and the most shifted potential to positive values, as shown in the inset A, which presents the dependences of the anodic and cathodic potentials on the applied charge (Q). The current for anodic and cathodic peaks for ferrocene are almost linearly decreasing with Q, as it can be seen in the inset B. This evolution is in agreement with the thickness of the film.

#### Study of **P2**

Experiments were carried out to characterize compound **P2**, similarly to the assays performed to characterize the compound **P1**. The CV and DPV curves have been recorded in **P2** solutions in 0.1 M TBAP, CH<sub>3</sub>CN. They are shown in Figure 11 for different concentrations (0 – 0.5 mM). DPV curves show five oxidation peaks (a1 – a5) and three reduction peaks (c1 – c3). One anodic peak (a1) and three cathodic peaks (c1, c2, c3) are seen in CV, denoted in agreement with processes notation from DPV curves. The peak currents are increasing with the concentration for both CV and DPV curves. In Figure 11 and Table 4 are given the linear plots of the peak currents on **P2** concentration for the main

peaks, and their equations and correlation coefficients, respectively. Good correlation coefficients have been obtained. The slopes in Table 4 indicate an increase of the peak height with **P2** concentration, with different slopes for the investigated peaks, as in the case of **P1**. The peak potentials from DPV and CV curves for **P2** are given in Table 5.

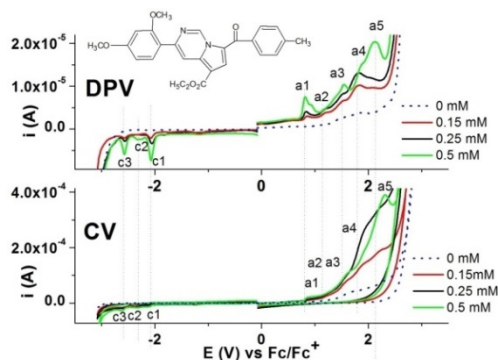


**Fig. 11.** CV (0.1 V·s<sup>-1</sup>) and DPV (0.01 V·s<sup>-1</sup>) curves on glassy carbon electrode (diameter 3 mm) at different concentrations for **P2** in 0.1 M TBAP/CH<sub>3</sub>CN

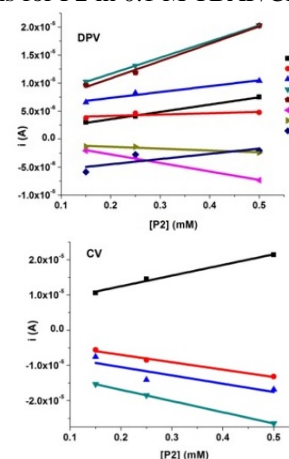


**Fig. 12.** Linear dependences of the peak currents on **P2** concentration from (a) DPV (0.01 V·s<sup>-1</sup>) and (b) CV (0.1 V·s<sup>-1</sup>) curves from Fig. 11

RDE anodic and cathodic curves at different rotation rates (500 - 2000 rpm) recorded for [P<sub>2</sub>] = 0.5 mM and the corresponding DPV curve are given in Fig.13. The curves present the isosbestic point (I1) situated at about 1.45 V. In the range of a<sub>2</sub> DPV peak, RDE currents have constant values, and they increase again in the range of a<sub>3</sub> process. These anodic RDE curves could be explained by the processes given in Table 5. The currents in the potential domain of a<sub>3</sub> are inversely proportional to the rotation rate, while those in the domains of a<sub>4</sub> and a<sub>5</sub> are almost not influenced by the rotation rate.

**Table 4.** Equations and the correlation coefficients of the linear peak currents dependences on concentration\* from CV (0.1 V·s<sup>-1</sup>) and DPV (0.01 V·s<sup>-1</sup>) curves from Fig. 11

Method	Equation*	Correlation coefficient
DPV	$i_{\text{peak a1}} = 0.95 + 13.1 \cdot [\text{P2}]$	0.994
	$i_{\text{peak a3}} = 5.26 + 10.6 \cdot [\text{P2}]$	0.941
	$i_{\text{peak a4}} = 5.89 + 28.8 \cdot [\text{P2}]$	0.999
	$i_{\text{peak a5}} = 4.65 + 30.92 \cdot [\text{P2}]$	0.986
	$i_{\text{peak c1}} = 0.31 - 15.2 \cdot [\text{P2}]$	0.996
	$i_{\text{peak c2}} = -0.71 - 3.33 \cdot [\text{P2}]$	0.894
CV	$i_{\text{peak a1}} = 6.41 + 30.2 \cdot [\text{P2}]$	0.984
	$i_{\text{peak c1}} = -2.81 - 21.0 \cdot [\text{P2}]$	0.978
	$i_{\text{peak c3}} = -10.6 - 31.8 \cdot [\text{P2}]$	0.999

\* $i_{\text{peak}}$  is expressed in  $\mu\text{A}$ , and  $[\text{P2}]$  in mmol/L

In Fig.14 are given the CV curves at different scan rates for the first anodic and cathodic peaks, and the linear dependences of their currents on the square root of the scan rate. High values of correlation coefficients have been obtained (Fig. 14b).

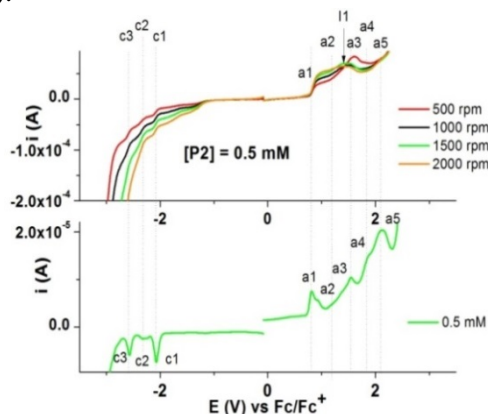


**Fig.13.** RDE curves (0.01 V·s<sup>-1</sup>) on glassy carbon electrode (3 mm diameter) at different rotation rates (500 – 2000 rpm) in 0.5 mM **P2** solution in 0.1 M TBAP/CH<sub>3</sub>CN (a); DPV curve obtained for 0.5 mM solution of **P2** on glassy carbon electrode (3 mm diameter) in 0.1 M TBAP/CH<sub>3</sub>CN (b)

In figure 15 are shown the CV curves of **P2** on different scan domains. The reversibility of each process has been estimated from these curves (Table 5). Processes obtained in the anodic domain are irreversible. Those from the cathodic domain are irreversible (c1) or quasi-reversible (c2, c3), with corresponding peaks situated at potentials shifted of 70 mV (for c2') and 100 mV (for c3') in respect with the peaks in the direct scans.

**Table 5.** Peak potentials values (V) vs Fc/Fc<sup>+</sup> from DPV and CV curves for **P2**

Peak	Method		Process characteristic
	DPV	CV	
a1	0.82	0.87	irreversible
a2	1.19	-	irreversible
a3	1.54	1.57	irreversible
a4	1.81	2.17	irreversible
a5	2.12	-	-
c1	-2.08	-2.12	irreversible
c2	-2.33	-2.33	quasi-reversible
c3	-2.57	-2.62	quasi-reversible

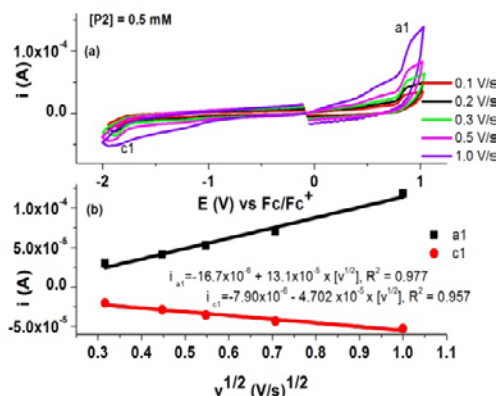


**Fig. 14.** CV curves in 0.1 M TBAP/CH<sub>3</sub>CN on glassy carbon electrode (3 mm diameter) for **P2** (0.5 mM) at different scan rates (0.1 – 1 V·s<sup>-1</sup>) (a) and dependences of the peak currents on the square root of the scan rate (b)

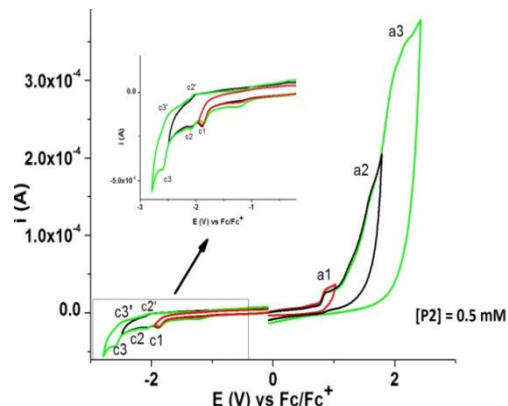


**Fig. 15.** CV curves (0.1 V·s<sup>-1</sup>) on glassy carbon electrode (3mm diameter) on different scan domains for **P2** (0.5 mM) in 0.1 M TBAP/CH<sub>3</sub>CN; inset: detail of the cathodic domain

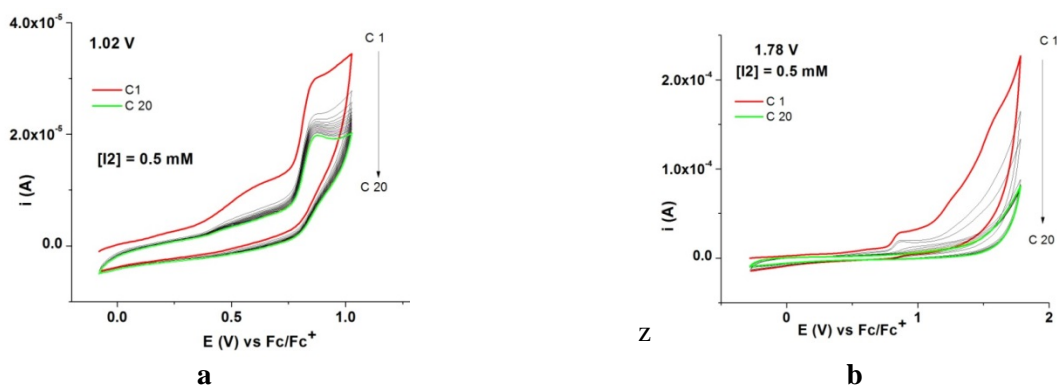


**Fig. 16.** CV curves ( $0.1 \text{ V}\cdot\text{s}^{-1}$ ) during the preparation of CMEs by successive scans in  $0.5 \text{ mM}$  solution of **P2** in  $0.1 \text{ M}$  TBAP,  $\text{CH}_3\text{CN}$  between  $-0.3 \text{ V}$  and different anodic limits:  $+1.02 \text{ V}$  (a);  $+1.78 \text{ V}$  (b)

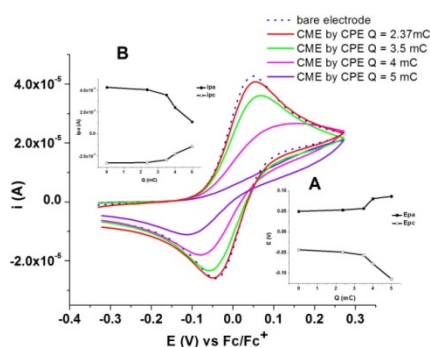


**Fig. 17.** CV curves ( $0.1 \text{ V/s}$ ) in  $1 \text{ mM}$  ferrocene solutions in  $0.1 \text{ M}$  TBAP,  $\text{CH}_3\text{CN}$  for the CME prepared in  $0.5 \text{ mM}$  **P2** solution in  $0.1 \text{ M}$  TBAP/ $\text{CH}_3\text{CN}$  by CPE at  $+1.78 \text{ V}$  at different charges  $Q$ ; dependences on  $Q$  of the anodic and cathodic Fc peak potentials (inset A) and currents (inset B)

#### Modified electrodes with **P2**

Chemical modified electrodes based on **P2** were obtained either by potentiodynamic or potentiostatic methods in solutions of **P2** ( $0.5 \text{ mM}$ ) in the domain of the anodic processes a1 and a2. In order to test that the electrode is covered, the modified electrodes were transferred in  $1 \text{ mM}$  ferrocene solution in  $0.1 \text{ M}$  TBAP,  $\text{CH}_3\text{CN}$ .

The modified electrodes were prepared by successive scans (20 cycles) between  $-0.3 \text{ V}$  and different anodic limits:  $1.02 \text{ V}$  (Figure 16 a);  $1.78 \text{ V}$  (Figure 16 b). The curves obtained after the transfer in ferrocene solution for anodic limits of  $1.02 \text{ V}$ , and  $1.78 \text{ V}$  are presented in Fig. 17. It can be seen that the ferrocene signal is much more flat in comparison to the bare electrode when the potential limit is more positive. The dependencies of the anodic and cathodic peak potentials for ferrocene (Fc) on the selected anodic limit scan are seen in Fig. 17 inset A; they show important changes starting at potentials more positive than  $1 \text{ V}$ . The corresponding anodic and cathodic currents dependencies, which indicate a sharp decrease after  $1 \text{ V}$ , are shown in Fig. 17 inset B.

Films based on **P2** have been also prepared by CPE at different potentials ( $1.02 \text{ V}$  and  $1.78 \text{ V}$ ); there were no important changes in ferrocene CV for charges of  $2.37 \text{ mC}$  or  $3.5 \text{ mC}$ . However, if CPE has been performed at  $1.78 \text{ V}$  evident changes occur continuously when the charge increases from  $2.37 \text{ mC}$  to  $5 \text{ mC}$ . In Fig. 17 are given the CV curves after the transfer in  $1 \text{ mM}$  ferrocene solution of the CMEs obtained at  $1.78 \text{ V}$  at different charges, indicating an increase with charge of the electrode coverage. Fig. 17 insets A and B show the dependences of ferrocene anodic and cathodic peak potentials and currents, respectively, on charge ( $Q$ ); after  $Q = 3.5 \text{ mC}$ , the anodic and cathodic potentials are sharply increasing with  $Q$ , while the currents are decreasing with  $Q$ .

#### Comparison between **P1** and **P2**

The diffusion coefficients for **P1** and **P2** have been calculated from the slopes of a1 peaks given in Figure 6 (b) and Figure 14 (b) using Randles–Sevcik equation (1), taking into account that the CV curves have been obtained at room temperature ( $298 \text{ K}$ ). In (1),  $i_p$  = peak current (A),  $n$  = number of electrons transferred in the redox process ( $n=1$ ),  $A$  = electrode area ( $\text{cm}^2$ ),  $D$  = diffusion coefficient ( $\text{cm}^2/\text{s}$ ),  $C$  = concentration of **P1** or **P2** ( $\text{mol}/\text{cm}^3$ ), and  $v$  = scan rate ( $\text{V}/\text{s}$ ). Compound **P2** has a higher diffusion coefficient (Table 6) than **P1**, in agreement with his small molecular volume.

$$i_p = 268600 \cdot n^{3/2} \cdot A \cdot C \cdot D^{1/2} \cdot v^{1/2} \quad (1)$$

**Table 6.** Diffusion coefficients for compounds **P1** and **P2**

Comp.	X	Slope	$10^5 \times D$ ( $\text{cm}^2/\text{s}$ )
<b>P1</b>		0.000068	10.2
<b>P2</b>		0.000131	19.1



It can be noticed from Figure 18 and Table 7 that compounds **P1** and **P2** have very close potentials for a1 and c1 peaks, as expected taking into account their similar structure.

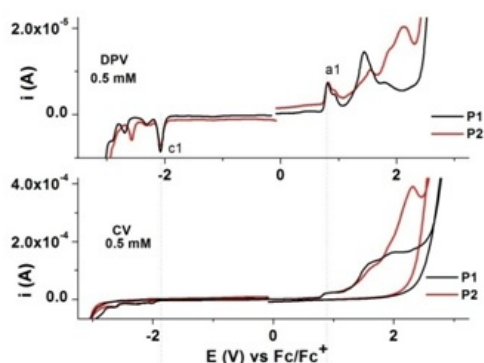


**Fig.18.** Comparison of DPV and CV curves in 0.1 M TBAP, CH<sub>3</sub>CN for **P1** (0.5 mM) and **P2** (0.5 mM)

**Table 7.** Peak potentials (V) from DPV curves (0.5 mM) and the assessed processes for **P1** and **P2**

Compound	<b>P1</b>	<b>P2</b>	Functional group/process
Peak			
a1	0.81	0.82	Py→Py <sup>+</sup> /oxidation 1*
a2	0.93	1.19	Ph / oxidation 2
a3	1.44	1.54	Py/oxidation 3
a4	1.80	1.81	Py/oxidation 4
a5	-	2.12	Py/oxidation 5
c1	-1.99	-2.08	CO→CO <sup>-</sup> →CHOH/reduction 1
c2	-2.23	-2.33	Pyrrole double bonds/reduction 2
c3	-2.61	-2.57	Ester/reduction 3
c4	-2.82	-	Pyrimidine/reduction 4

\*= pyrrolo[1,2-c]pyrimidine moiety

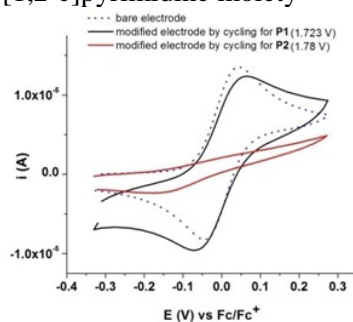


**Fig. 19.** CV curves (0.1 V·s<sup>-1</sup>) in 1mM ferrocene solutions in 0.1 M TBAP, CH<sub>3</sub>CN on modified electrodes prepared by 20 scans between -0.3 V and 1.723 V for **P1** and 1.78 V for **P2**, and on bare electrode (dotted line), respectively

## CONCLUSIONS

The electrochemical characterization of ethyl 3-(2,4-dimethoxyphenyl)-7-(2-naphthoyl)pyrrolo [1,2-c]pyrimidine-5-carboxylate (**P1**) and ethyl 3-(4-methylphenyl)-7-(4-methylbenzoyl)pyrrolo [1,2-c]pyrimidine-5-carboxylate (**P2**) was performed by cyclic voltammetry, differential pulse voltammetry and rotating disk electrode methods.

The pyrrolo[1,2-c]pyrimidines present similar peaks in the anodic and cathodic domain. Modified

Pyrrolo[1,2-c]pyrimidine has a low aromatic character, which confers a high reactivity in comparison to the common aryls. The difficulty of peak assessment is increased by the presence of stabilizing functional groups, which have redox potentials close to the aromatic moiety. The potentials of DPV peaks and the assessed processes for the compounds **P1** and **P2** are presented in Table 7.

The transfer in ferrocene solution (Figure 19) of the modified electrodes based on **P1** and **P2**, obtained by successive cycling between -0.3 V and about 1.7 V, lead to more distorted curves in case of **P2**, indicating that **P2** covers better the electrode surface, probably due to the formation of a more compact film.

electrodes were obtained by successive scanning or by controlled potential electrolysis at different anodic peaks and charges. The coverage of the electrode surface was confirmed by the transfer of the modified electrodes in ferrocene solutions, when the CV signal for ferrocene was found attenuated in intensity and distorted (with an increased gap between the peak potentials). **P2** gave the best electrode coverage by electrooxidation. The modified electrodes investigation is in progress in view of OLED applications.

**Acknowledgements:** The authors are grateful for the financial support from: Executive Agency for Higher Education, Research, Development and Innovation Funding (UEFISCDI) project ID PN-II-RU-TE-2014-4-0594 contract no. 10/2015, PN-II-PT-PCCA-2013-4-2151 contract no. 236/2014, and Romania–China bilateral project 68BM/2016 (CH 41.16.04).

## REFERENCES

1. F. Rise, H. Wikstroem, S. Ugland, D. Dijkstra, L.L. Gundersen, P. De Boer, A. Bast, G. Haenen, O.G. Antonsen, WO 9621662 A1 (1996).
2. M. Ono, L. Sun, Z.Q. Xia, E. Kostik, K. Koya, Y. Wu, M. Nagai, Fused pyrrole compounds, WO 2004082606 A2 (2004).
3. G. Mangalagiu, M. Ungureanu, G. Grosu, I.I. Mangalagiu, M. Petrovanu, *Ann. Pharm. Fr.*, **59**, 139 (2001).
4. S. Kristafor, T.G. Kraljevic, S.M. Ametamey, M. Cetinac, I. Ratkajd, R.T. Haceke, S. K. Pavelic, S. R. Malic, *Chem. Biodivers.*, **8**, 1455 (2011).
5. J.T. Kim, A.D. Hamilton, C.M. Bailey, R.A. Domoal, L. Wang, K.S. Anderson, W.L. Jorgensen, *J. Am. Chem. Soc.*, **128**, 15372 (2006).
6. M.A. Ibrahim, S.M. Abou-Seri, M.M. Hanna, M.M. Abdalla, N.A.E. Sayed, *European Journal of Medicinal Chemistry*, **99**, 1 (2015).
7. M. Ono, L. Sun, Z.Q. Xia, E. Kostik, K. Koya, Y. Wu, M. Nagai, *Intl. Pat. WO 2004/082606*.
8. G. Mangalagiu, M. Ungureanu, G. Grosu, I.I. Mangalagiu, M. Petrovanu, *Annales pharmaceutiques françaises*, **59**, 139 (2001).
9. E. Georgescu, F. Georgescu, P. C. Iuhas, C. Draghici, M. G. Danila, P. I. Filip, *Arkivoc*, **381**, 242 (2007).
10. J.M. Minguez, J.J. Vaquero, J.L. Garcia-Navio, J. Alvarez-Builla, *Tetrahedron Lett.*, **37**, 4263 (1996).
11. M. Alvarez, D. Fernandez, J.A. Joule, *J. Chem. Soc. Perkin Trans.*, **1**, 249 (1999).
12. V. B. Ivanov, V. S. Reznik, B. E. Ivanov, A. A. Musina, Efremov, Yu. Ya., *Izv. Akad. Nauk. SSSR, Seriya Khim.*, 2428 (1980).
13. C.H. Weidner, F.-M. Michaels, D. J. Beltman, C.J. Montgomery, D.H. Wadsworth, B. T. Briggs, L.M. Picone, *J. Org. Chem.*, **56**, 5594 (1991).
14. A. Copar, B. Stanovnik, M. Tisler, *J. Heterocycl. Chem.*, **30**, 1577 (1993).
15. Y. N. Romashin, M.T.H. Liu, S.S. Nijjar, O. Attanasi, *Chem. Commun.*, 1147 (2000).
16. A. De la Hoz, J.L.G. De Paz, E. Diez-Barra, J. Elguero, C. Pardo, *Heterocycles*, **24**, 3473 (1986).
17. G.C. Mangalagiu, I.I. Mangalagiu, R.I. Olariu, M. Petrovanu, *Synthesis*, **14**, 2047 (2000).
18. C.C. Moldoveanu, I.I. Mangalagiu, *Helv. Chim. Acta*, **88**, 2747 (2005).
19. I.I. Mangalagiu, G.C. Mangalagiu, C. Deleanu, G. Drochioiu, M.G. Petrovanu, *Tetrahedron*, **59**, 111 (2003).
20. E. Georgescu, F. Georgescu, M.M. Popa, C. Draghici, L. Tarko, F. Dumitrascu, *ACS Combi Sci.*, **14**, 101 (2012).
21. E. Georgescu, F. Georgescu, C. Draghici, L. Cristian, M.M. Popa, F. Dumitrascu, *Comb Chem High T Scr*, **16**, 851 (2013).
22. L. Soare, E.-M. Ungureanu, E. Georgescu, L. Birzan, *REV. CHIM. (Bucharest)*, **63**, 1451 (2012).
23. B. W. D. Andrade, S. Datta, S. R. Forrest, P. Djurovich, E. Polikarpov, M. E. Thompson, *Organic Electronics*, **6**, 11 (2005).

## ЕЛЕКТРОХИМИЧНИ ИЗСЛЕДВАНИЯ НА ДВА ПИРОЛ [1,2-с] ПИРАМИДИНИ

М.-Л. Тату<sup>1</sup>, Ф. Харя<sup>1</sup>, Е.-М. Унгуреану<sup>1\*</sup>, Е. Джорджеску<sup>2</sup>, Л. Бирзан<sup>3</sup>, М.-М. Попа<sup>3</sup>

<sup>1</sup>Катедра по неорганична химия, физикохимия и електрохимия, Университет "Политехника" на Букурещ, 011061, Румъния

<sup>2</sup>Научен център Олтхим, 240050, Ramnicu Valcea, Румъния,

<sup>3</sup>Румънска академия, Институт по органична химия "С. Д. Ненитческо", 060023-Букурещ, Румъния

Постъпила на 25 август, 2017 г.; приета на 18 септември, 2017 г.

(Резюме)

Електрохимичното охарактеризиране на два пирол [1,2-с] пиримидини е извършена чрез циклична волтаметрия (CV), диференциална импулсна волтаперометрия и волтаперометрия с ротиращ дисков електрод. Техните дифузионни коефициенти са определени на основа влиянието, което оказва скоростта на сканиране на потенциала върху CV анодните токове. Модифицираните електроди са приготвени в пирол [1,2-с] пиримидинови разтвори в ацетонитрил, съдържащ тетрабутиламониев перхлорат чрез циклиране на потенциала или чрез контролирана потенциална електролиза при различни анодни потенциали и заряди.

**Ключови думи:** пирол [1,2-с] пиримидини, циклична волтаперометрия, диференциална импулсна волтаперометрия, дифузионни коефициенти, модифицирани електроди, ротиращ дисков електрод